Dalton Transactions

ROYAL SOCIETY OF CHEMISTRY

PAPER

View Article Online
View Journal | View Issue

Cite this: *Dalton Trans.*, 2025, **54**, 14025

A tight binding pocket in photoluminescent N^C^N cyclometalated Pt(II), Pd(II), and Ni(II) complexes

Maryam Niazi, [a] Iván Maisuls, [b,c] Cristian A. Strassert, *[b,c] Pablo González-Herrero [d] and Axel Klein *[a]

In the frame of our research aiming to develop efficient triplet-emitting materials, we are exploring the role of the second coordination sphere in enhancing the rigidity of structures and its controlling aspect over the extents of excited state distortions. We thus synthesised three N^C^N cyclometalated complexes [M(L^{Bn})Cl] (M = Pt, Pd, and Ni), where the two *ortho*-positions of the pyridyl moieties in 1,3-di(2-pyridyl)-benzene are benzyl substituted (Bn) forming a tight binding pocket for the metal and the Cl^- ancillary ligand. The molecular structures from single-crystal X-ray diffraction show a markedly distorted square planar M(II) coordination with τ_4 values of around 0.4. UV-vis absorption spectra show long-wavelength bands in the range 350 to 5400 nm with the energies increasing along the series Ni < Pt < Pd. The Pt(II) complex emits in solution at 298 K (λ_{max} = 544 nm) and displays aggregated emission within poly(methyl methacrylate) (PMMA) films at various concentrations at 298 K. The Pd(II) derivative exhibits a broad emission band at 77 K in a frozen glassy 2-MeTHF matrix, peaking at 530 nm. Very different from the Pt(II) and Pd(II) spectra, the Ni(II) sample showed a broad emission with λ_{max} = 699 nm at 77 K, with a quantum yield of 20% and ms lifetime. TD-DFT calculated decomposition of the assumed emissive T_1 state showed similar ^{3}MLCT character of about 30% for all three complexes, but marked differences in LC character of about 38% for Pd and Pt and only 5% for Ni. In turn, for Ni the by far the highest MC character (42%) was calculated which strongly speaks against triplet photoluminescence from the Ni(II) complex.

Received 12th June 2025,
Accepted 21st August 2025

DOI: 10.1039/d5dt01385b

rsc.li/dalton

Introduction

Luminescent organometallic transition metal complexes with efficient photophysical properties are widely explored for applications such as optoelectronics,[1–6] photocatalysis,[7–9] and optical sensors.[10–12] In contrast to the abundance of well-known square-planar Pt(II) complexes with emissive properties,[1–8,11–17] the number of reported Pd(II) complexes with similar emissive characteristics is notably lower,[18–23] with even fewer examples observed for Ni(II) complexes.[23–29] From a photophysical perspective, key challenges arise due to the smaller spin–orbit coupling (SOC) and weaker ligand field, which lead to energetically low-lying metal-centred (^{3}MC) excited states with respect to the electronic ground state.[29–32] This is problematic, as the thermal population of ^{3}MC states would result in fast non-radiative deactivation.[27,33–36] Another significant concern, regardless of the type of the metal, stems from the structural distortion encountered by the triplet (T_1) excited state relative to the singlet (S_0) ground state. This distortion leads to the vibronic coupling of the T_1 and S_0 states, ultimately causing rapid radiationless relaxation from the T_1 state. The impact of this structural distortion is evident even in Pt(II) complexes featuring tridentate cyclometalating ligands, which inherently possess a stronger ligand field, yet still experience detrimental effects on their luminescence properties.[13,37–40] Hence, the design of the ligands/coordination environment, modulates the structural and photophysical properties. In 2014, a series of Pt(II) complexes featuring a doubly cyclometalating C^N^C ligand with phenyl and bulky carboranyl fragment was reported. These complexes display high luminescence quantum yields (Φ_L), reaching approximately 82% at ambient temperature, which is attributed to the suppression of non-radiative relaxation facilitated by their rigid molecular structure.[13] [Ni(dpb)(carbazolate)] (Hdpb = 1,3-di-(2-pyridyl)-benzene; Scheme 1) has been reported as the first phosphorescent cyclometalated Ni(II) complex, exhi-

[a]*University of Cologne, Faculty for Mathematics and Natural Sciences, Department of Chemistry and Biochemistry, Institute for Inorganic and Materials Chemistry, Greinstrasse 6, D-50939 Köln, Germany. E-mail: mniazi1@smail.uni-koeln.de, axel.klein@uni-koeln.de; Tel: +49-221-470-4006*
[b]*Universität Münster, Institut für Anorganische und Analytische Chemie, Corrensstr. 28/30, D-48149 Münster, Germany*
[c]*CeNTech, CiMIC, SoN, Heisenbergstr. 11, D-48149 Münster, Germany. E-mail: maisuls@uni-muenster.de, cstra_01@uni-muenster.de*
[d]*Departamento de Química Inorgánica, Facultad de Química, Universidad de Murcia, Campus de Espinardo 19, 30100 Murcia, Spain. E-mail: pgh@um.es*

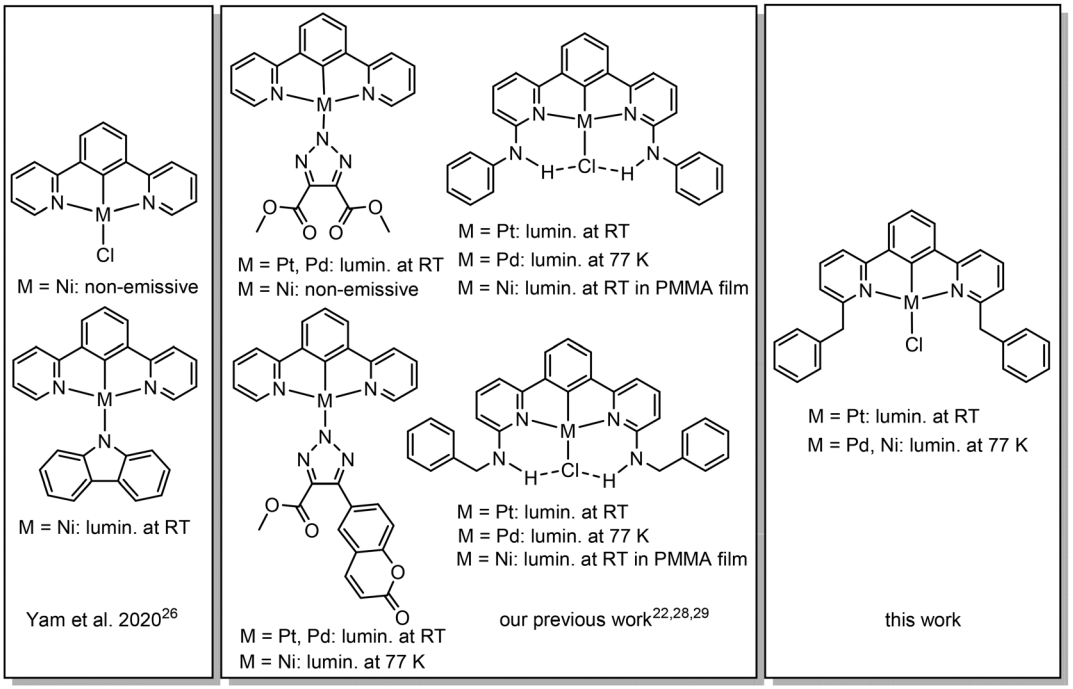

Scheme 1 Previously reported Ni(II), Pd(II), Pt(II) dpb complexes and scope of this report.

biting weak photoluminescence in the solid state at room temperature, with an emission band peaking at 468 nm at 77 K.[26] The emission was assigned to a metal-perturbed ligand-centred (^{3}LC or π–π^*) excited state.[26] In contrast, the parent complex, [Ni(dpb)Cl], was found to be non-emissive. The emission properties of [Ni(dpb)(carbazolate)] were attributed to the incorporation of a strong σ-donating carbazolyl ligand at the Ni(II) centre, which suppresses the influence of low-lying ^{3}MC excited state that would otherwise lead to non-radiative decay.[26] A study on excited-state relaxation of ^{3}MLCT states in Ni(II) complexes reported varying lifetimes (τ) including 0.5 ps for [Ni(bib)(CH_3CN)]PF_6, 17 ps for [Ni(bib)(Ln^2)](PF_6) and 48 ps for [Ni(bib)(Ln^1)](PF_6) (H_3bib = 1,3-bis(3′-butylimidazolyl-1′-yl)benzene; Ln^1 and Ln^2: isocyanide ligands with a *m*-terphenyl backbone) in aerated CH_2Cl_2 at 20 °C.[27] The findings suggest that the tridentate H_3bib ligand (C^C^C) and steric-protecting ancillary ligands offer a promising approach to counteract the unwanted distortions in square-planar coordination throughout the excited state relaxation pathway.

Recent investigations into cyclometalated [M(dpb)X] complexes (M = Pt, Pd, and Ni; X = triazolato^{COOCH_3,COOCH_3} or triazolato^{Coumarin,COOCH_3}; Scheme 1) have provided further insight into their photophysical behaviour.[28] While Pd(II) and Pt(II) complexes exhibit luminescence originating from metal-perturbed ^{3}LC excited states, Ni(II) derivative with triazolato^{COOCH_3,COOCH_3} coligand remain non-emissive at both room and low temperatures. This non-radiative behaviour is attributed to the presence of an accessible S_1/S_0 conical intersection, which facilitates efficient deactivation to the ground state. Notably, [Ni(dpb)(triazolato^{Coumarin,COOCH_3})] deviates from this trend, displaying phosphorescence from the T_5 state in frozen glassy matrix at 77 K (λ_{em} = 472 nm, τ = 147.8 μs).[28]

In our recent studies,[22,29] we explored how non-covalent interactions within the second coordination sphere influence the photophysics of d^8-configured metal complexes of Ni(II), Pd(II), and Pt(II). Specifically, the introduction of NHR substituents into [M(L^{NHR})Cl] complexes, where L^{NHR} represents N^C^N cyclometalating dipyridyl-phenide ligands with NH(C_6H_5) (L^{NHPh}) and NH($CH_2C_6H_5$) (L^{NHBn}), resulted in NH···Cl···NH hydrogen bonds, acting akin to molecular locks (Scheme 1). This approach of locking ligands minimised the usually occurring geometry distortion between the S_0 and T_1 states, enabling Ni(II) derivatives to exhibit phosphorescence in frozen glassy matrices at 77 K and in poly(methyl methacrylate) (PMMA) matrix in the temperature range between 6 K and 300 K, with Φ_L values exceeding 30% at 77 K.[22,29]

Building upon our earlier findings,[22,29] our objective was to assess how the rigidity of the structures would be affected by replicating the steric bulk of the coordination environment without the presence of NH···Cl···NH hydrogen bonds. Herein, we report on the syntheses, structural characterisation, and photophysical properties of three cyclometalated complexes [M(L^{Bn})Cl] (M = Pt, Pd, and Ni) with the bis-3-benzyl substituted dpb ligand (Scheme 1).

Experimental section

Materials

Dry THF was obtained from distillation over Na/K alloy. [Ni(COD)$_2$] (COD = 1,5-cyclooctadiene) was obtained as previously

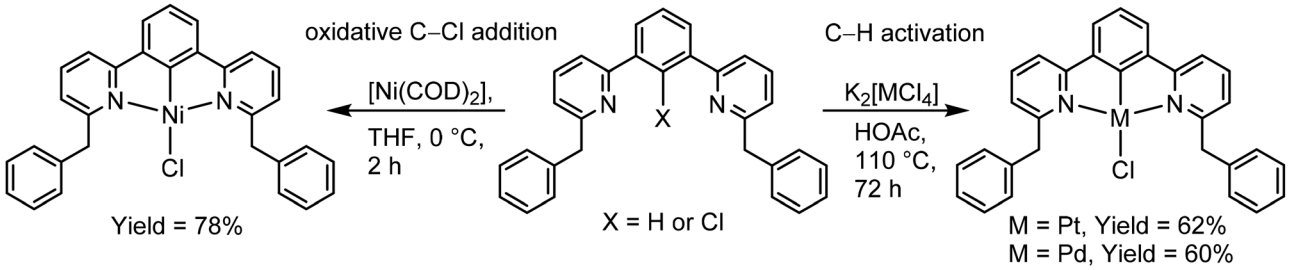

Scheme 2 Syntheses of the Ni(II), Pd(II), and Pt(II) complexes.

reported.[32] All other chemicals were used as received. The ligand precursors HL^{Bn} and ClL^{Bn} were synthesised through Suzuki cross coupling reactions in 82% and 72% yield (Scheme 2, details in the SI).

Syntheses

Synthesis of the Pt(II) and Pd(II) complexes – general description. Modifying a previously reported method,[41] a mixture of 1.0 eq. $K_2[PtCl_4]$ or $K_2[PdCl_4]$ and 1.0 eq. of the proto-ligand HL^{Bn} was suspended in 8 mL glacial acetic acid and stirred at 110 °C for 3 d. The crude products were filtered off, washed sequentially with glacial acetic acid, MeOH, H_2O, EtOH, and Et_2O. Further purification was done by crystallising the products in DMSO and washing the crystals with cold acetone and then *n*-pentane.

[Pt(L^{Bn})Cl]. From $K_2[PtCl_4]$ 0.180 g (0.44 mmol) and HL^{Bn} 0.181 g (0.44 mmol). Yield 0.175 g (0.27 mmol, 62%) orange-yellow solid. ^{1}H NMR (600 MHz, DMSO-d_6, 298 K): δ = 8.03 (t, J = 7.7 Hz, 2H, H7), 7.97 (dd, J = 7.9, 1.6 Hz, 2H, H8), 7.70 (d, J = 7.7 Hz, 2H, H3), 7.44–7.40 (m, 4H, H12), 7.38 (dd, J = 7.7, 1.5 Hz, 2H, H6), 7.29 (t, J = 7.7 Hz, 1H, H4), 7.24–7.19 (m, 4H, H13), 7.19–7.15 (m, 2H, H14), 5.27 (s, 4H, H10). ^{13}C NMR (151 MHz, DMSO-d_6, 313 K): δ = 165.93 (C9), 165.65 (C5), 140.95 (C2), 139.95 (C7), 139.27 (C11), 128.96 (C12), 128.45 (C13), 126.18 (C14), 125.05 (C6), 124.78 (C3), 123.35 (C4), 117.44 (C8), 43.36 (C10), 40.06 (C1). HR-ESI MS(+): calcd for $[C_{30}H_{23}N_2Pt]^+$ m/z = 605.14823; found m/z = 605.14855 $[M - Cl]^+$. Elemental analysis calcd (%) for $C_{30}H_{23}ClN_2Pt$, M = 642.05 g mol^{-1}: C, 56.12; H, 3.61; N, 4.36. Found C, 56.44; H, 3.65; N, 4.46.

[Pd(L^{Bn})Cl]. From $K_2[PdCl_4]$ 0.160 g (0.49 mmol) and HL^{Bn} 0.202 g (0.49 mmol). Yield 0.163 g (0.29 mmol, 60%) yellow solid. ^{1}H NMR (600 MHz, DMSO-d_6, 298 K): δ = 8.02 (t, J = 7.8 Hz, 2H, H7), 7.95 (dd, J = 7.9, 1.4 Hz, 2H, H8), 7.69 (d, J = 7.7 Hz, 2H, H3), 7.44–7.39 (m, 4H, H12), 7.32 (dd, J = 7.7, 1.4 Hz, 2H, H6), 7.29 (t, J = 7.7 Hz, 1H, H4), 7.26–7.23 (m, 4H, H13), 7.22–7.18 (m, 2H, H14), 5.04 (s, 4H, H10). ^{13}C NMR (151 MHz, DMSO-d_6, 313 K): δ = 164.90 (C9), 163.11 (C5), 143.21 (2), 140.22 (7), 139.27 (C11), 128.99 (C12), 128.51 (C13), 126.26 (C14), 125.05 (C4), 125.01 (C6), 124.81 (C3), 117.32 (C8), 43.22 (C10), 40.06 (C1). HR-ESI MS(+): calcd for $[C_{30}H_{23}N_2Pd]^+$ m/z = 516.09065; found m/z = 516.09156 $[M - Cl]^+$. Elemental analysis calcd (%) for $C_{30}H_{23}ClN_2Pd$, M = 553.39 g mol^{-1}: C, 65.11; H, 4.19; N, 5.06. Found C, 65.33; H, 4.21; N, 5.17.

Synthesis of the Ni(II) complex

Under an inert atmosphere, 0.355 g (0.79 mmol, 1.0 eq.) of the ClL^{Bn} ligand precursor was dissolved in 12 mL of dry THF. The reaction mixture was transferred in an ice bath at 0 °C and 0.284 g (1.3 mmol, 1.3 eq.) of $[Ni(COD)_2]$ was added. The solution turned from yellow to orange with red-orange precipitation during 2 h. Then the solvent was removed and the residue was washed with dry MeCN to remove unreacted ligand and dried under vacuum. Yield 0.313 g (0.62 mmol, 78%) deep orange solid. ^{1}H NMR (300 MHz, DMSO-d_6, 298 K): δ = 7.90 (t, J = 7.7 Hz, 2H, H7), 7.80 (dd, J = 7.9, 1.4 Hz, 2H, H8), 7.58 (d, J = 7.6 Hz, 2H, H3), 7.49–7.39 (m, 4H, H12), 7.34–7.19 (m, 7H, H6 and H4 and H13), 7.02 (dd, J = 7.6, 1.4 Hz, 2H, H14), 4.64 (s, 4H, H10). HR-ESI MS(+): calcd for $[C_{30}H_{23}N_2Ni]^+$ m/z = 469.12092; found m/z = 469.12076 $[M - Cl]^+$. Elemental analysis calcd (%) for $C_{30}H_{23}ClN_2Ni$, M = 505.66 g mol^{-1}: C, 71.26; H, 4.58; N, 5.54. Found C, 71.18; H, 4.61; N, 5.57.

Instrumentation

^{1}H and ^{13}C spectra were recorded on a Bruker Avance II 300 MHz (^{1}H: 300 MHz, ^{13}C: 75 MHz) equipped with a double resonance (BBFO) 5 mm observe probe head with *z*-gradient coil, Bruker Avance III 500 MHz (^{1}H: 500 MHz, ^{13}C: 126 MHz), and Bruker Avance II 600 MHz spectrometer (^{1}H: 600 MHz, ^{13}C: 151 MHz) with a triple resonance (TBI) 5 mm inverse probe head with *z*-gradient coil using a triple resonance (Bruker, Rheinhausen, Germany). The unambiguous assignment of the ^{1}H and ^{13}C resonances was obtained from ^{1}H NOESY, ^{1}H COSY, ^{1}H ^{13}C HSQC, and ^{1}H ^{13}C HMBC experiments. All 2D NMR experiments were performed using standard pulse sequences from the Bruker pulse program library. Chemical shifts were measured relative to TMS (^{1}H, ^{13}C). UV-vis absorption spectra were recorded on *Varian* Cary 05E spectrophotometer (Varian Medical Systems, Darmstadt, Germany). Elemental analyses were obtained using a *HEKAtech* CHNS EuroEA 3000 analyser (HEKAtech, Wegberg, Germany). HR-ESI-MS(+) spectra were measured at the Thermo Scientific LTQ OrbitrapXL mass spectrometer *via* electrospray ionisation and a FTMS Analyser. EI-MS spectra in the positive mode were measured using a *Finnigan* MAT 95 mass spectrometer. Simulations were performed using ISOPRO 3.0. Electrochemical measurements were carried out in 0.1 M

n-Bu_4NPF_6 solution in THF (tetrahydrofuran) using a three-electrode configuration (glassy carbon electrode, Pt counter electrode, Ag/AgCl reference) and a Metrohm Autolab PGSTAT30 or μStat400 potentiostat (Metrohm, Filderstadt, Germany). The potentials were referenced against the ferrocene/ferrocenium redox couple as internal standard.

Photophysical measurements

Steady-state excitation and emission spectra were recorded on a FluoTime 300 spectrometer from PicoQuant (Berlin, Germany) equipped with a 300 W ozone-free Xe lamp (250–1100 nm), a 10 W Xe flash-lamp (200–1100 nm, pulse width *ca.* 1 μs) with repetition rates of 0.1 to 300 Hz, a double-grating excitation monochromator (Czerny-Turner type, grating with 1200 lines per mm, blaze wavelength: 300 nm), diode lasers (pulse width < 20 ps) operated by a computer-controlled laser driver PDL-828 "Sepia II" (repetition rate up to 80 MHz, burst mode for slow and weak decays), two emission monochromators (Czerny-Turner, selectable between double-grating blazed at 500 nm with 2.7 nm mm^{-1} dispersion and 1200 lines per mm, or single-grating blazed at 1200 nm with 5.4 nm mm^{-1} dispersion and 1200 lines per mm, or single-grating blazed at 1250 nm with 5.4 nm mm^{-1} dispersion and 600 lines per mm) with adjustable slit width between 25 μm and 7 mm, and Glan-Thompson polarisers for excitation (after the Xe-lamps) and emission (after the sample). Different sample holders (Peltier-cooled mounting unit ranging from −15 to 110 °C or and adjustable front-face sample holder), along with two detectors (namely a PMA Hybrid-07 from PicoQuant with transit time spread FWHM < 50 ps, 220–850 nm, or a H10330C-45-C3 NIR detector with transit time spread FWHM 0.4 ns, 950 to 1400 nm from Hamamatsu) were used. Steady-state and photoluminescence lifetimes were recorded in TCSPC mode by a PicoHarp 300 instrument (minimum base resolution 4 ps) or in MCS mode by a TimeHarp 260 (where up to several ms can be traced). Emission and excitation spectra were corrected for source intensity (lamp and grating) by standard correction curves. For samples with lifetimes in the ns order, an instrument response function calibration (IRF) was performed using a diluted Ludox® dispersion. Lifetime analysis was performed using the commercial EasyTau 2 software (PicoQuant). The quality of the fit was assessed by minimising the reduced chi squared function (χ^2) and visual inspection of the weighted residuals and their autocorrelation. All solvents used were of spectrometric grade (Uvasol®, Merck). Photoluminescence quantum yields were measured with a Hamamatsu Photonics absolute PL quantum yield measurement system (C9920-02) equipped with a L9799-01 CW 150 W Xenon light source, a monochromator, a C7473 photonic multi-channel analyser, an integrating sphere and employing U6039-05 software (Hamamatsu Photonics). All cuvettes used were round quartz cuvettes and the solvents were of spectrometric grade (Uvasol®, Merck).

Time-resolved multiphoton micro(spectro)scopy was performed using a fluorescence microscope (IX 73 from Olympus) equipped with a complete confocal system, a laser combining unit (LCU), an inverted microscope body, and a multichannel detection unit (Multiharp 150, PicoQuant) equipped with diode lasers. These lasers provide adjustable output power and repetition rates up to 80 MHz, all within a compact fiber-coupled unit with wavelengths between 375 to 640 nm. A FLIMbee galvo scanner is positioned between the main optical unit (MOU) and the microscope to achieve extremely stable scanning speeds while maintaining high positioning precision, enabling applications ranging from fast fluorescence lifetime imaging (rapidFLIM) to phosphorescence lifetime imaging measurements (PLIM). For beam diagnostics, a charge-couple device (CCD) camera and a photodiode are available in the MOU of the microscope. The MOU is equipped with two detectors: a hybrid photomultiplier-based single photon counting module (PMA Hybrid 40, PicoQuant) and a SPAD-based photon counting module (SPCM-AQR-14, PerkinElmer). Depending on the emission of the sample, various band-pass (BP) and low-pass (LP) filters were placed in front of these detectors as needed to acquire lifetime maps. Data acquisition was conducted using the unique time-tagged time-resolved (TTTR) measurement mode, allowing for simultaneous data acquisition on two channels. Data were processed and analysed with the SymphoTime 64 (PicoQuant) software. To couple the MicroTime 200 and the FluoTime 300 instruments, a fibre coupler was employed, enabling the spectrometer to record either steady-state or time-resolved luminescence spectra and decays from a sample mounted on the microscope. Luminescence micrographs were acquired using the aforementioned microscope, equipped with a X-CiteQ Lamp module (Excelitas Technologies) as excitation source and a UI-5580SE (IDS) digital camera. Depending on the photophysical properties of the sample, different band pass (BP) and low pass (LP) cubes were using accordingly.

Crystal structure determination

X-ray diffractometry (XRD) measurements were carried out at 100(2) K using Bruker D8 Venture diffractometer including a Bruker Photon 100 CMOS detector with Mo Kα (λ = 0.71073 Å) radiation. The data was collected using APEX4 v2021.10-0.[42] The structures were solved through dual space methods using SHELXT and Olex2, and refined with SHELXL 2017 and SHELXL 2018/2019 employing full-matrix least-squares methods on $F_0^2 \geq 2\sigma(F_0^2)$.[43–45] The non-hydrogen atoms were refined with anisotropic displacement parameters without any constraints. The hydrogen atoms were included by using appropriate riding models. The $[Ni(L^{Bn})Cl]\cdot\frac{1}{2}CH_2Cl_2$ structure was refined omitting an observed slight disorder of CH_2Cl_2. Including the disorder did not result in a better refinement. For $[Pt(L^{Bn})Cl]$, the largest hole density (−2.0 e $Å^{-3}$) is located in a non-chemically significant position. Trials to reduce this were unsuccessful and we thus rule out an artefact from structure solution or refinement, but ascribe this problem to an artefact in the raw data. Data of the structure solutions and refinements can be obtained for CCDC 2307143 ($[Pt(L^{Bn})Cl]$), CCDC 2271328 ($[Pd(L^{Bn})Cl]$) and CCDC 2258876 ($[Ni(L^{Bn})Cl]\cdot\frac{1}{2}CH_2Cl_2$).

Computational details

All DFT calculations were performed using the Gaussian 16 suite of programs.[46] For all atoms, def2-TZVP basis sets, as well as the corresponding def2-ECPs for Pt and Pd (ecp-46 and ecp-28) were used for the core electrons.[47,48] The S_0 and T_1 geometries of all compounds were optimised with the hybrid functional TPSSh, using Grimmes D3 dispersion correction and the conductor-like polarisable continuum model (CPCM) parametrised for THF as solvation model.[49–53] Geometry optimisation was followed by frequency calculations and yielded no imaginary modes, thus confirming the energetically minimal nature of the stationary points. For the TD-DFT calculated UV-vis absorption spectra, the 45 lowest excited singlet states were calculated at the optimised S_0 geometry. Molecular orbitals and electronic properties were extracted from single point calculations. The TD-DFT calculation output was further evaluated using the software package TheoDORE to analyse relative MLCT, LMCT, LC, LL'CT, (L = N^C^N, L′ = Bn) and MC contributions to the emissive T_1 states, using the implemented standard algorithm for molecular partitioning of transition metal complexes employing Openbabel.[54]

Results and discussion

Syntheses and characterisation

The ligand precursors HL^{Bn} and ClL^{Bn} were synthesised through Suzuki cross coupling reactions in 82% and 72% yield. The Pt(II) and Pd(II) complexes $[M(L^{Bn})Cl]$ were synthesised from $K_2[MCl_4]$ (M = Pt or Pd) and HL^{Bn} through the established method of heating in glacial acetic acid,[41] in 62% and 60% yield (Scheme 2). The Ni(II) complex was obtained by modifying an established procedure[55] including oxidative addition reaction of $[Ni(COD)_2]$ (COD = 1,5-cyclooctadiene) with the chlorinated ligand precursor ClL^{Bn} in 78% yield (Scheme 2). The Pt(II) (yellow), Pd(II) (pale yellow), and Ni(II) (orange-red) complexes were characterised by nuclear magnetic resonance (NMR) spectroscopy (Fig. S1 to S14, SI), high-resolution electrospray mass spectrometry (HR-ESI-MS) (Fig. S14, SI), elemental (CHN) analyses, and single-crystal X-ray diffraction (sc-XRD). The three complexes are insoluble in non-polar solvents but are soluble in polar solvents, though the Ni(II) derivative must be handled under the exclusion of air and moisture (Fig. S15, SI).

Experimental crystal structures and DFT-calculated molecular structures

The three compounds were crystallised from saturated CH_2Cl_2 solutions. $[M(L^{Bn})Cl]$ (M = Pt or Pd) crystallised isostructural in the triclinic space group $P\bar{1}$, while $[Ni(L^{Bn})Cl]\cdot\frac{1}{2}CH_2Cl_2$ was solved in the monoclinic space group $C2/c$ and includes half a molecule of CH_2Cl_2 per formula unit (Fig. S16 to S18, data in Tables S1 and S2, SI). The experimental data for the complexes were used to benchmark our Density Functional Theory (DFT) geometry-optimisation using TPSSh/def2-TZVP/CPCM(THF) with good agreement between the experimental and calculated metrics (Fig. S19, Table S2, SI).

The crystal structures feature long metal···metal distances ranging from 5.106(1) Å for the Ni complex to 6.123(1) Å for the Pt and 6.125(1) Å for the Pd complexes. They are far beyond the sum of van der Waals radii; thus, no significant metallophilic M···M interactions were found. All the structures showed pronounced π-stacking between the pyridine and phenyl units of two neighbouring molecules with centroid distances ranging from 3.52 Å for the Pt and Pd complexes to 3.62 Å for the Ni complex (Fig. S16 to S18, SI).

Very similar to our recently reported $[M(L^{NHR})Cl]$ (R = Ph or Bn, M = Pt, Pd, and Ni) complexes,[22,29] the three $[M(L^{Bn})Cl]$ complexes show marked distortion of the Cl^- coligand out of the square planar coordination plane (Fig. 1), resulting in τ_4 values ranging from 0.35 to 0.44. The τ_4 index is calculated as the sum of the two largest angles (α and β) around the four-coordinate metal centres, subtracted from 360°, and divided by 141° (360 − 2 × (109.5)°). A value of $\tau_4 = 0$ corresponds to a perfect square planar geometry, and $\tau_4 = 1$ to a perfect tetrahedral geometry.[56]

The deviation of the C–M–Cl angle from the ideal 180° is higher for the Ni complex (138.5(3)°) compared with the Pd (150.3(1)°) and Pt (152.1(1)°) derivatives. This is connected with shorter Ni–C1 (1.811(8) Å) and Ni–Cl (2.320(3) Å) bonds relative to the Pd and Pt analogues (Table S2, SI).

Generally, the τ_4 values for these new series of complexes are bigger than those reported for the $[M(L^{NHR})Cl]$ (R = Ph or Bn, M = Pt, Pd, and Ni) complexes[22,29] by about 0.1 which is in line with an increased steric bulk of the binding pocket.

So, replacing the NHR groups of our previous complexes[22,29] through benzyl substituents on the N^C^N ligand scaffold proves the negligible role of the M–Cl···H–N hydrogen bonding in the complexes on the deviation from planar and emphasise on the importance of the steric bulk of the *ortho*-substituents as already predicted by the DFT-calculated $[M(L^{OMe})Cl]$ complexes.[22,29] This deviation along with the experimentally observed structural trends in the solid state are well reproduced by the DFT-optimised structures.

DFT-optimised S_0 and T_1 geometries

The DFT-optimised S_0 geometries of the complexes generally exhibit good agreement with the experimental data from crystallography, displaying maximum deviations of 0.03 Å and 2.4° for individual distances or angles (Table S2, SI). In the T_1 excited state the C–M–Cl angles, constituting a significant portion of the observed distortion in the S_0 state, experience further deviation (Fig. 2, data in Table S2). This phenomenon is particularly pronounced for Pt(II) and Pd(II), where angles of 121.7 and 114.6°, respectively were found in the T_1 state compared to 154.0° (Pt) and 149.4 (Pd) the S_0 state. For Ni(II), the increase of deviation is less pronounced as already the S_0 geometry shows a value of 139.2°, which is further reduced to 121.6° in the T_1 state. This goes along with an elongation of the M–C in all three cases, but larger M–N distances only for Pd and Ni (Table S2). At the same time, other critical metrics surrounding the metal atoms exhibit minimal changes,

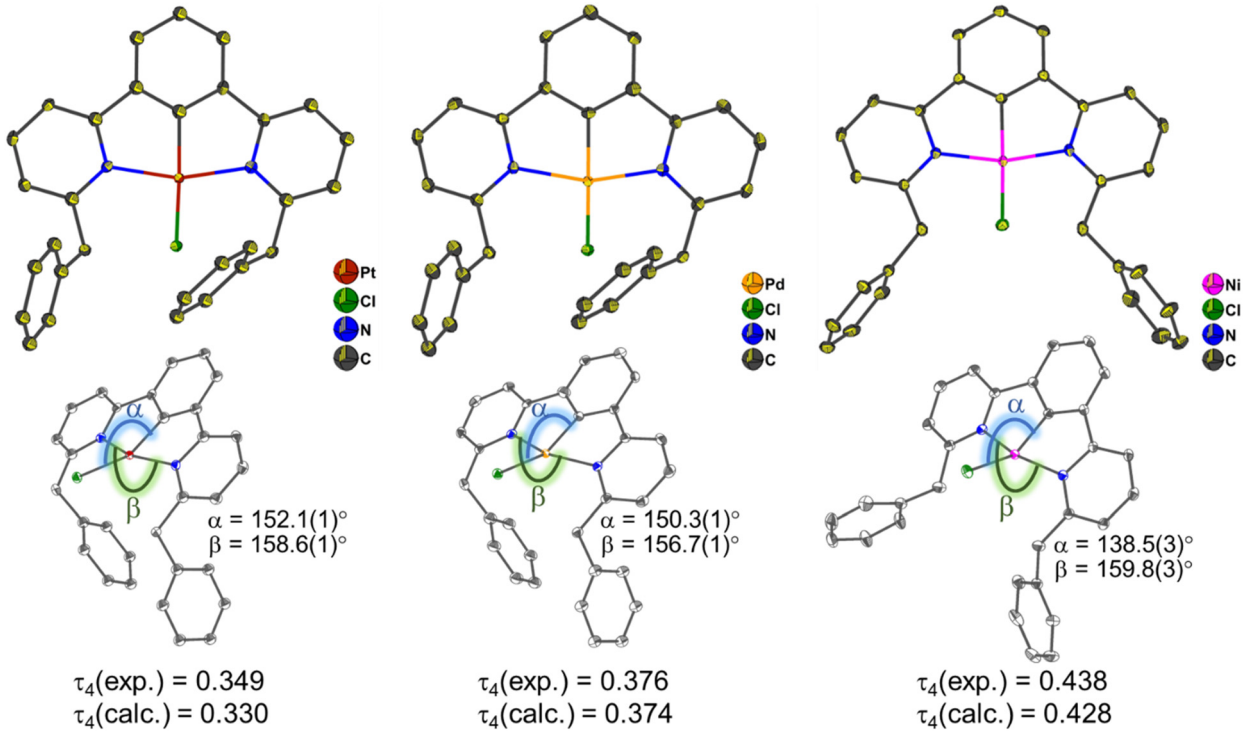

Fig. 1 Molecular structures of the complexes [M(L^{Bn})Cl] (M = Pt, Pd, and Ni) from single crystal X-ray diffraction (top, 50% displacement ellipsoids) and their side-on views featuring the deviation τ_4 from the square planar coordination (bottom).

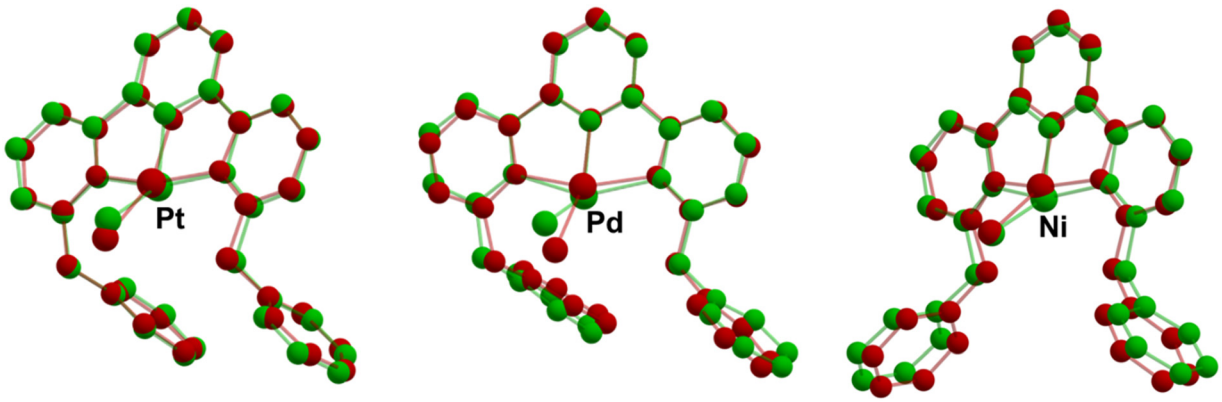

Fig. 2 DFT-calculated geometries of [M(L^{Bn})Cl] (M = Pt, Pd, Ni) in the S_0 (red) and T_1 (green) states.

especially with the pyridyl and phenyl rings of the cyclometalated L^{Bn} ligand remaining coplanar in the complexes.

Electrochemistry and DFT-calculated frontier molecular orbitals

Cyclic voltammograms showed a first irreversible reduction wave at around −2.30 V for Pt(II) and Pd(II) complexes and at −2.15 V for Ni(II) derivatives, *vs.* the ferrocene/ferrocenium couple (Fig. 3, full data in Table S3, SI; cyclic voltammograms are presented in Fig. S20, SI). The first wave is usually followed by a second and third irreversible reduction wave at potentials ranging from −2.41 V to −3.11 V. The first reduction potentials are very similar to the NHR substituted complexes for R = phenyl but slightly less negative when compared to the NHR substituted complexes with R = benzyl. Other reported M(dpb) complexes (Table 1)[14,22,29,57,59] lie in the same range and remarkably to not allow a simple correlation of the reduction potentials with the substitution pattern on the dpb ligand.

The DFT-calculated lowest unoccupied molecular orbitals (LUMO) show predominant π*-character of the N^C^N ligand core and the energies of −2.38 for Pt(II) and −2.35 eV for Pd(II) are very similar and only slightly higher (less negative) than the −2.30 eV calculated for the Ni(II) derivative (Fig. S21 and Table S5, SI). We thus assign the reduction processes as essen-

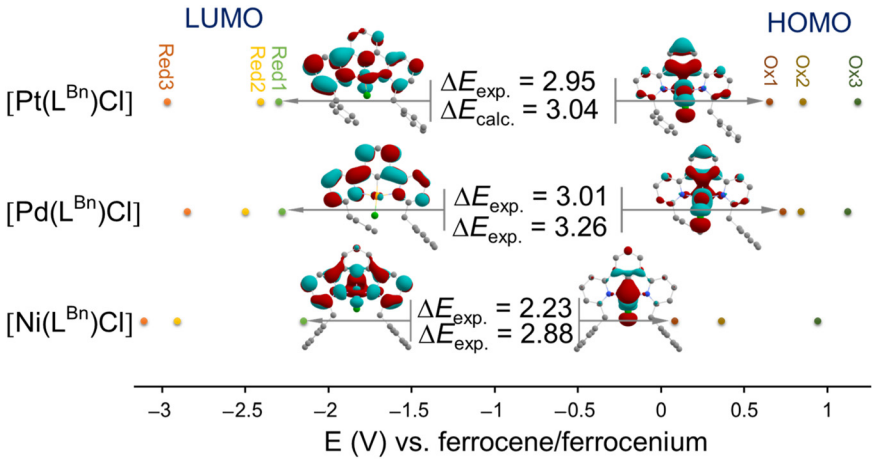

Fig. 3 Selected experimental redox potentials (dots) and HOMO–LUMO gaps ($\Delta E_{exp.}$) from cyclic voltammetry together with DFT-calculated HOMO and LUMO compositions and HOMO–LUMO gaps ($\Delta E_{calc.}$) for the complexes [M(L^{Bn})Cl] (M = Pt, Pd, and Ni).

Table 1 Selected redox potentials of the [M(L^{Bn})Cl] complexes and comparable derivatives[a]

Complex	*E* Red1	*E* Ox1	Δ*E* (Ox1–Red1)	Solvent
[Pt(L^{Bn})Cl]	−2.30 i	0.65	2.95	THF
[Pd(L^{Bn})Cl]	−2.28 i	0.73	3.01	THF
[Ni(L^{Bn})Cl]	−2.15 i	0.08	2.23	THF
[Pt(L^{NHPh})Cl][b]	−2.29 r	0.93	3.22	THF
[Pd(L^{NHPh})Cl][b]	−2.31 r	0.95	3.26	THF
[Ni(L^{NHPh})Cl][c]	−2.17 i	0.06	2.23	THF
[Pt(L^{NHBn})Cl][b]	−2.45 r	0.90	3.35	THF
[Pd(L^{NHBn})Cl][b]	−2.43 r	0.95	3.38	THF
[Ni(L^{NHBn})Cl][c]	−2.38 i	0.13	2.51	THF
[Pt(Me_2dpb)Cl][d]	−2.24 r	0.35	2.59	THF
[Pd(Me_2dpb)Cl][d]	−2.34 r	0.74	3.07	THF
[Ni(Me_2dpb)Cl][d]	−2.26 i	0.10	2.36	THF
[Pt(dpb)Cl][e]	−2.14 r	0.35	2.49	MeCN
[Ni(dpb)Cl][f]	−2.33 i	0.06	2.39	THF

[a] From cyclic voltammetry in *n*-Bu_4NPF_6/THF. Potentials in V *vs.* ferrocene/ferrocenium; accuracy of potentials: ±0.003 V. Half-wave potential for reversible processes (marked with r), cathodic peak potentials for irreversible reductions (i), *E* Ox1: anodic peak potentials for irreversible oxidations. Full data in Table S3, SI. [b] From ref. 22. [c] From ref. 29. [d] From ref. 59. [e] From ref. 14. [f] From ref. 57.

tially taking place at the ligand, in line with results for similar M(dpb) complexes.[57–60]

On the anodic side, a first irreversible oxidation wave at 0.65 V for Pt(II), 0.73 V for Pd(II), and 0.08 V for Ni(II) are recorded (Fig. S20 and Table S3, SI). Potentials for the corresponding NHR-substituted Pt(II) and Pd(II) derivatives are slightly higher (Table 1).[22] Compared with [Ni(L^{Bn})Cl], the NHR-substituted complexes gave a slightly lower oxidation potential for R = Ph (0.06 V) and a markedly higher potential for R = benzyl (0.13 V, Table 1). While the lower potentials for the L^{Bn} complexes of Pt(II) and Pd(II) compared with those carrying the NHR-substituted ligands is in line with the electron-withdrawing effect of the amino function, the situation for the Ni(II) derivative might be governed by both electronic and steric effects in line with the finding that the phenyl derivative [Ni(L^{HPh})Cl] shows a higher τ_4 value of 0.352 compared with the L^{HBn} derivative with 0.332, both markedly lower than τ_4 for [Ni(L^{Bn})Cl] of 0.428 (calculated values).

The DFT-calculated highest occupied molecular orbital (HOMO) for the [M(L^{Bn})Cl] complexes gain essential contributions from the metals and the central aryl group with some contributions from the benzyl groups and the Cl^- coligand (Fig. S21, Table S5, SI). The calculated HOMO energies are increasing from Pd (−5.62 eV) to Pt (−5.62), to Ni (−5.18 eV). The predominant metal contributions agree with M^{II}/M^{III}-based oxidation processes and are in line with previous reports.[23,59–62]

The electrochemical gaps Δ*E* (Ox1–Red1) increase along the series Ni < Pt < Pd and thus qualitatively agree well with the calculated HOMO–LUMO gaps (Fig. 3). The same behaviour was also reported for the series of [M(Me_2dpb)Cl] and [M(N^C^N)Cl] (N^C^N = L^{NHPh} or L^{NHBn}, M = Pt, Pd, and Ni) complexes (Table 1). A comparison between the parent/unsubstituted [Pt(dpb)Cl] and the Me-substituted [Pt(Me_2dpb)Cl] complexes reveals a slightly increase in the reported HOMO–LUMO gap for the [Pt(L^{Bn})Cl] complex by 0.46 and 0.36 V, respectively. Conversely, when compared to [Pt(L^{NHBn})Cl] and [Pt(L^{NHPh})Cl] complexes, the HOMO–LUMO gap for [Pt(L^{Bn})Cl] decreases by 0.4 and 0.27 V, respectively (Table 1). For [Pd(L^{Bn})Cl], this gap value decreases by 0.06, 0.25, and 0.37 V compared to [Pd(Me_2dpb)Cl], [Pd(L^{NHPh})Cl], and [Pd(L^{NHBn})Cl] complexes, respectively. Interestingly, the HOMO–LUMO gap for [Ni(L^{Bn})Cl] matches that of [Ni(L^{NHPh})Cl], but decreases by 0.13, 0.16, and 0.28 V when compared with [Ni(Me_2dpb)Cl], [Ni(dpb)Cl], and [Ni(L^{NHR})Cl] complexes, respectively (Table 1).

UV-vis absorption and photoluminescence spectra with TD-DFT-calculated electronic transitions

The UV-vis absorption spectra of the complexes [M(L^{Bn})Cl] (M = Pt, Pd, and Ni) feature intense bands in the UV-range of up

to 308 nm. Since they also occur for the ligand precursors HL^{Bn} and ClL^{Bn}, we can assign them to transitions into excited singlet states with $^1\pi$–π^* (^{1}LC) character (Fig. 4, data in Table S4, SI). They are followed by medium intensity, structured absorption bands down to almost 570 nm. For the Ni(II) complex, the long-wavelength absorption band show a maximum at 433 nm, which tails down to a cut-off at 518 nm (Fig. 4). For the Pt(II) complex, the maximum is blue-shifted to 421 nm and the cut-off shifts to 453 nm. For the Pd(II) derivative, the maximum is even more blue-shifted to 381 nm and the cut-off appears at 403 nm. When taking these cut-off energies into account, an increasing series of the optical HOMO–LUMO gaps Ni (2.39 eV) < Pt (2.74 eV) < Pd (3.07 eV) is observed. The electrochemical HOMO–LUMO gaps follow the same series, *i.e.* Ni (2.23 eV) < Pt (2.95 eV) < Pd (3.01 eV) and are slightly smaller in case of Ni and Pd as expected. But the is opposite was found for the Pt complex with the electrochemical gap being larger than the optical gap by 0.21 eV. We have recently reported the same phenomenon for the Pt(II) complexes [Pt(C^N^C)($PnPh_3$)] (HC^N^CH = 2,6-diphenyl-pyridine or dibenzoacridine; Pn = P, As, Sb, or Bi) and rationalised this in terms of ^{3}MLCT contributions to the states associated with the lowest energy absorption bands, as based on TD-DFT and transient absorption (TA) spectroscopic studies.[63]

A closer look reveals low energy absorption bands with very low intensities at 496 nm for the Pt(II) complex (Fig. 4, data in Table S4, SI). The same features have been previously reported for [Pt(Me_2dpb)Cl] at 480 nm and [Pt(dpb)Cl] at 485 nm.[14,15,59] They are discussed as ^{3}MLCT contributions to the adsorption, promoted by the large spin–orbit coupling making the spin-forbitten $S_0 \rightarrow T_n$ transitions partially allowed,[14,15,28,63] which is in keeping with our above discussion on controversial finding that the optical gap of this Pt(II) complex is smaller than the electrochemical gap. When comparing the [M(L^{Bn})Cl] (M = Pt, Pd, and Ni) complexes with their NHR (R = phenyl or benzyl) substituted counterparts,[22,29] only a minimal effect on the absorption energies, approximately 10 nm, is observable.

TD-DFT calculated absorption spectra match qualitatively well with the experimental results (Fig. 4, Fig. S22, Tables S4 and S7, SI). They show low-energy absorption bands at 448 nm (Pt), 422 nm (Pd), and 424 nm with a broad shoulder at 501 nm (Ni) which are slightly red-shifted if compared with the experimental maxima (421, 381, 433 nm). Long-wavelength bands in three complexes have been previously assigned to transitions into mixed ligand-centred (^{1}LC)/metal-to-ligand charge transfer (^{1}MLCT) states as supported by the calculations and in keeping with previous reports.[14–16,22,29,59–63] Additionally, the long-wavelength maximum of the Ni(II) complex appear at lower energies compared to those of Pt(II) and Pd(II) derivatives, as corroborated by TD-DFT calculated spectra. This observation aligns with the lower experimental and DFT-calculated HOMO–LUMO gaps.

Photoluminescence spectroscopy revealed that the Pt(II) derivative is emissive at room temperature (RT) in both argon-purged CH_2Cl_2 solution and in the solid state (Fig. S23, S24 and Table S8, SI). The emission of the Pt(II) complex in fluid CH_2Cl_2 solution remained unchanged across the concentration range $c = 10^{-5}$, 10^{-6}, and 10^{-7} M. To investigate the formation of aggregates or excimers, the Pt(II) complex was incorporated into PMMA matrices at different concentrations. Increasing the concentration of PMMA matrices from 0.5% to 5% caused a red shift in the emission maximum from 496 nm to 544 nm, with corresponding changes in the emission profile, which closely resembled the spectrum recorded in CH_2Cl_2 solution and in the solid state at RT (Fig. S25 and Table S8, SI). These data suggest the presence of emissive molecular aggregates

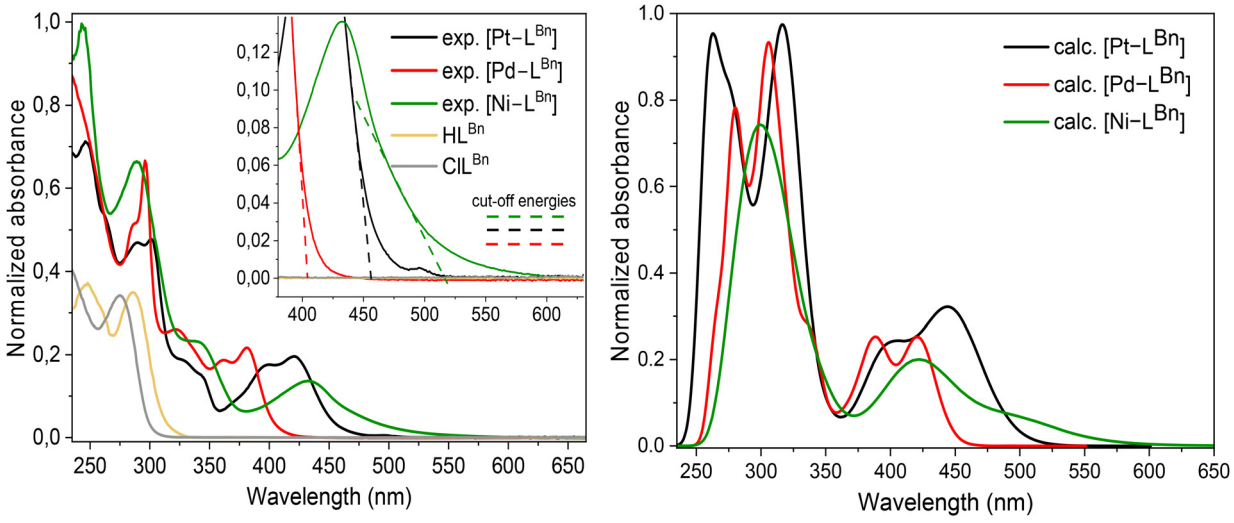

Fig. 4 Left: Experimental normalised UV-vis absorption spectra of the complexes [M(L^{Bn})Cl] (M = Pt, Pd, and Ni) in THF solution at 298 K (left) with a zoom into the long-wavelength region and dashed lines to illustrate the determination of the cut-off energies. Right: TD-DFT calculated spectra (right).

with increasing concentration in the PMMA matrices, indicating that the Pt(II) complex may emit primarily from aggregates in both the solid state and CH_2Cl_2 solution.

The Pd(II) and Ni(II) complexes were not emissive at RT. This is attributed to the population of dissociative metal-centred (MC) (d–d*) states, which provide non-radiative deactivation channels *via* conical intersections with the ground state. Consequently, these complexes are non-emissive in fluid solutions at RT. This outcome aligns with existing literature on such complexes, particularly for Pd(II) and Ni(II) complexes,[22,24,58,59,62] where the spin–orbit coupling (SOC) of Pd (1412 cm^{-1}) and Ni (630 cm^{-1}) is significantly smaller than that of Pt (4052 cm^{-1}).[64] However, at 77 K, samples of both complexes become emissive (Fig. 5). At this lower temperature, the thermal population of the d–d* states becomes inaccessible, and the rigidification of the system prevents non-radiative vibrational pathways and/or solvent quenching. While this effect is somehow expected in both Pt(II) and Pd(II) complexes, it is surprising that in the case of Ni(II), we found not only a defined emission spectrum, but also a high quantum yield (20%) along with lifetimes in the millisecond range (Table 2).

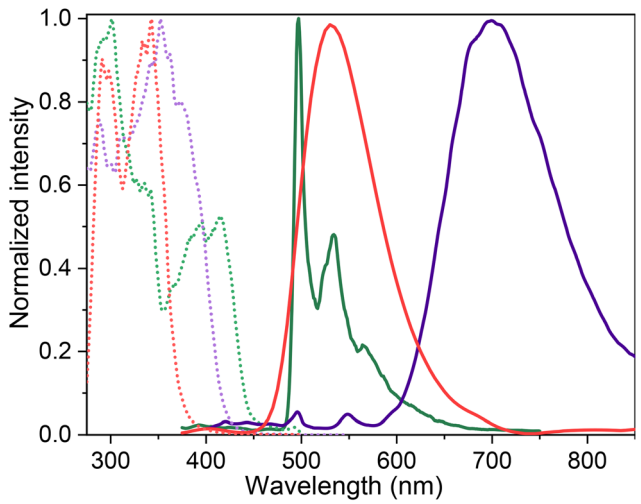

Fig. 5 Photoluminescence emission (dashed lines) and excitation (dotted lines) spectra of the complexes [M(L^{Bn})Cl] (M = Pt: green, Pd: red) in 2-MeTHF at 77 K as a glassy matrix (λ_{ex} = 350 nm) along with the spectrum obtained for the Ni(II) sample (violet) under the same conditions.

The Pt(II) complex shows an emission spectrum with a defined vibrational progression (λ_{max} = 497 nm) which is typical for such [Pt(N^C^N)X] complexes.[14,21,22,24,28,29,57–59] In contrast, the Pd(II) complex shows a broad, red-shifted emission band (λ_{max} = 530 nm). The different behaviour of the Pd(II) complex, compared with the Pt(II) derivative, is attributed to the emission from weakly coupled aggregates rather than monomeric species. The monomer emission is probably quenched by the solvent.[19,20,23] It is important to note that the emission spectrum did not change upon varying the concentration of the complex in the glassy matrix (from 10^{-4} to 10^{-7} M) indicating that this is not concentration-related phenomenon but rather an outcome of orientation of the complexes within the glassy matrix at 77 K. Generally, both the Pt(II) and the Pd(II) complex show features that are rather common for such complexes.[14,15,19,21–23,28] We conclude that although the spectra look slightly different, the excited states responsible for the emission can be described as having mixed contributions of ^{3}LC and ^{3}MLCT character in both cases.

For the sample of the Ni(II) complex, a relatively broad emission band peaking at λ_{max} = 699 nm was observed. The notably high photoluminescence quantum yield of 20% coupled with the lifetimes in the ms range point to a triplet nature of the emissive state.[28,29] However, for the light Ni(II) atom a marked metal-centred (MC) character if the emissive state could be expected from comparison with the previously studied non-luminescent [Ni(dpb)Cl],[24–26] with ps excited-

Table 2 Photophysical properties of [M(L^{Bn})Cl] (M = Pt, Pd, and Ni) complexes[a]

Compound	Φ_L ± 2%	τ_i [b] (μs)	k_r (10^4 s^{-1})	k_{nr} (10^4 s^{-1})
Pt(II)	10	τ_1 = 6.50 ± 0.06 (42%) τ_2 = 2.71 ± 0.05 (58%) τ_{av_amp} = 4.30 ± 0.01	2.3 ± 0.5	21.0 ± 0.5
Pd(II)	3	τ_1 = 205 ± 2 (64%) τ_2 = 100 ± 4 (36%) τ_{av_amp} = 167.5 ± 0.4	n.d.	0.57 ± 0.01
Ni(II)	20	τ_1 = 87 000 ± 1000 (27%) τ_2 = 9300 ± 200 (73%) τ_{av_amp} = 30 000 ± 500	(0.67 ± 0.08) × 10^{-3}	(3.00 ± 0.08) × 10^{-3}
HL^{Bn}	n.d.	τ_1 = 0.0073 ± 0.0002 (5%) τ_1 = 0.00146 ± 0.00001 (95%) τ_{av_amp} = 0.00177 ± 0.00002	n.d.	n.d.
ClL^{Bn}	n.d.	τ_1 = 0.0083 ± 0.0001 (9%) τ_1 = 0.00225 ± 0.00004 (91%) τ_{av_amp} = 0.00278 ± 0.00003	n.d.	n.d.

[a] Photoluminescence quantum yields (Φ_L) and lifetimes (τ) in frozen glassy 2-MeTHF matrices at 77 K, radiative k_r and non-radiative k_{nr} rate constants. [b] For multiexponential decays, the amplitude-weighted average lifetimes τ_{av_amp} are given. n.d. = not determined. Raw time-resolved photoluminescence decays and fitting parameters are shown in Fig. S28 to S35, SI.

states decay found in transient absorption spectroscopy (TAS) experiments.[24] On the other hand, the recently reported [Ni(dpb)X] complex (X = triazolato^{Coumarin,COOCH_3}; Scheme 1) showed phosphorescence (λ_{em} = 472 nm) from the T_5 state in frozen glassy matrix at 77 K and a lifetime τ of 147.8 μs was reported.[28] For the [Ni(L^{NHR})Cl] complexes, containing the NH(C_6H_5) (L^{NHPh}) and NH($CH_2C_6H_5$) (L^{NHBn}) substituted dpb ligand (Scheme 1), very long-lived emissions even in the ms time-domain were found, along with a short-lived component in the ns range.[29] The TD-DFT-based assignment of the excited state of the [Ni(L^{NHR})Cl] complexes to a triplet T_5 state is challenged by the intrinsic instability of the complexes.[29] Although the herein reported [Ni(L^{Bn})Cl] complex is far more stable than the L^{NHR} derivatives, we studied the ligand precursors HL^{Bn} and ClL^{Bn}, to ensure that the emission does not originate from residual ligand, the ligand precursors were measured at 77 K. Neither the emission spectra nor the lifetimes resemble those of the complexes (Fig. S26, S34, and S35 SI; data in Table 2). Nevertheless, we cannot rule out that the emission stems from decomposition products. UV-vis absorption spectroscopy (Fig. S15) showed that the complex decomposed within 400 min with marked changes already after 20 min. Irradiation of such solutions did not lead to accelerated decomposition, so we assign the decomposition to hydrolysis but can rule out photodecomposition. Irradiation of the glassy frozen samples at 77 K did also not show any sign of photo-decomposition on the samples. So, we can only tentatively assign this emission to the intact Ni(II) complex.

By means of the quantum yields and lifetimes, both the radiative and radiationless rate constants were calculated following eqn (1) and (3). Absolute uncertainties were estimated by eqn (2) and (4).

$$k_r = \frac{\Phi_L}{\tau_{av}} \quad (1)$$

$$\Delta k_r = \left(\frac{\Delta\Phi_L}{\tau_{av}}\right) + \left(\frac{\Delta\tau_{av}}{{\tau_{av}}^2} \cdot \Phi_L\right) \quad (2)$$

$$k_{nr} = \frac{1-\Phi_L}{\tau_{av}} \quad (3)$$

$$\Delta k_{nr} = \left(\frac{\Delta\Phi_L}{\tau_{av}}\right) + \left(\frac{(1+\Phi_L)\Delta\tau_{av}}{{\tau_{av}}^2}\right) \quad (4)$$

As observed in Table 2, by going down in the group a tendency is observed, where when going from Pt(II) to Ni(II), both k_r and k_{nr} decrease, which can be correlated with the far weaker spin–orbit coupling of Ni(II).[64]

By means of photoluminescence lifetime microscopy imaging (PLIM), both the decay rates and the phosphorescence spectra of the crystalline phase of the Pt(II) complex was measured. The corresponding lifetime maps and emission spectra of the crystal are shown in Fig. 6. As expected, both Pd(II) and Ni(II) crystals did not show any measurable luminescence at ambient temperature.

The character of the assumed emissive T_1 states for all three complexes was assessed through excitation analysis using the TheoDORE package[53] (Fig. 7). The decomposition into MLCT (d–π*), ligand-to-metal-charge-transfer (LMCT), ligand'-to-ligand-charge-transfer (L'LCT), LC (π–π*), and metal-centred (MC) contributions is based on the partitioning of the

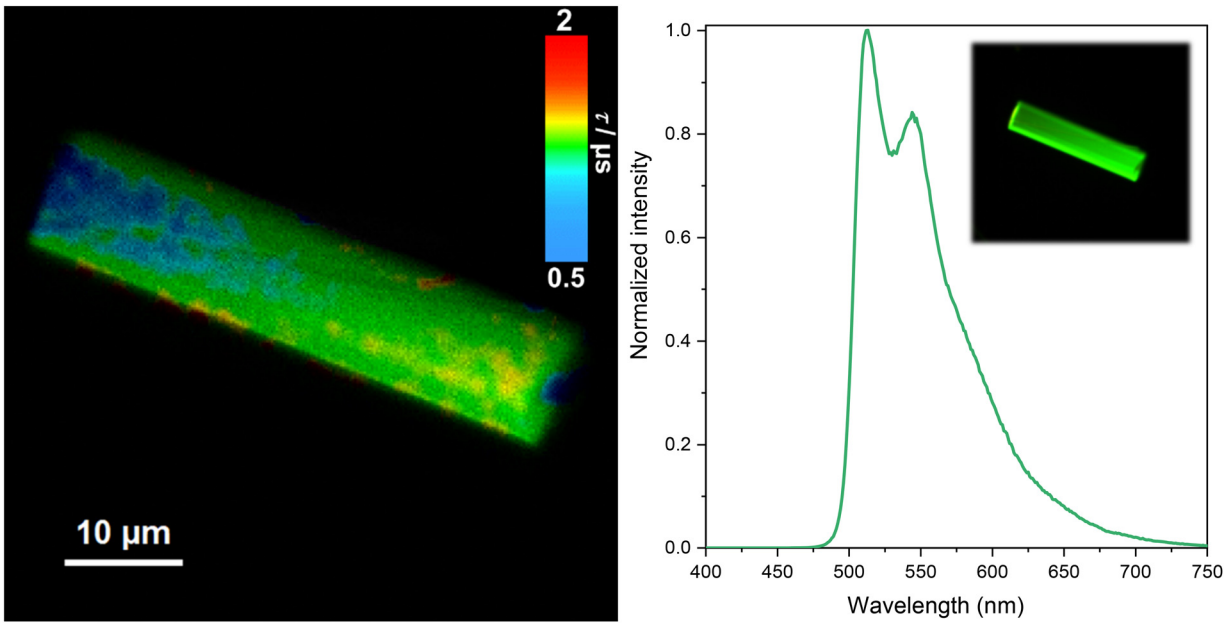

Fig. 6 Time resolved photoluminescence micro(spectro)scopy imaging of the Pt(II) complex in a single crystal at 298 K. Left: Photoluminescence lifetime map of the crystalline phase of the complex (λ_{ex} = 376 nm, low-pass cut-off filter 514 LP). Right: Photoluminescence spectrum of the single crystal measured with the microscope, inset: photoluminescence micrograph. Raw time-resolved photoluminescence decays can be seen in Fig. S30, SI.

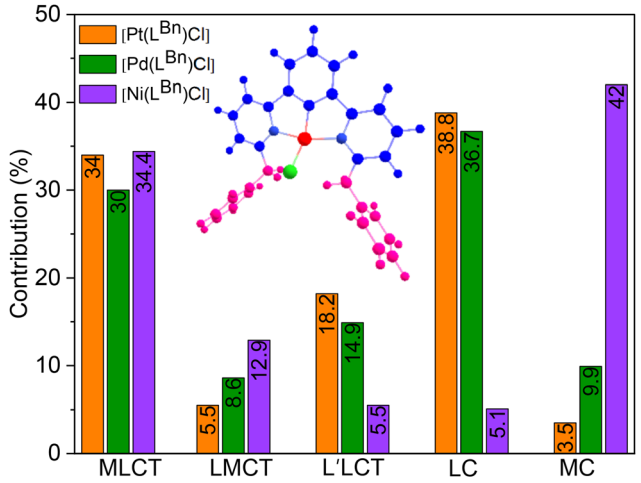

Fig. 7 Decomposition of the T_1 state for the three calculated complexes into contributions originating from MLCT, LMCT, LC, L'LCT, or MC configurations determined with the package TheoDORE,[54] together with the partitioning of the [M(L^{Bn})Cl] complexes for the numerical analysis. L'LCT describes ligand-centred transitions between different parts of the tridentate ligand, while LC represents excitation within the same part.

complexes as defined in Fig. 7. The MLCT character for [Ni(L^{Bn})Cl] and [Pt(L^{Bn})Cl] are virtually the same (34%) and higher as for [Pd(L^{Bn})Cl] (30%). For the Pt and Pd derivatives, the LC character is superior with about 38% compared with 5% calculated for the Ni derivative, that admixes by far the highest MC character (42%). The L'LCT character decreases down the series from Pt to Ni, while the LMCT contribution increases.

The findings for the Pt(II) and Pd(II) complexes are quite similar to what has been reported for comparable complexes.[19,22–24,28,39,62,63] The high MLCT character of the T_1 of the Ni(II) derivative is a good argument for the assumption that the observed emission stems from the complex, while the high MC character speaks strongly against this, as such a state should lead to rapid radiationless decay. The question why we presumably observe photoluminescence from this complex, despite this high MC character, might lie in the dynamics at low temperatures, combined with the peculiar geometric distortion of the complex in both ground and excited states. The rapid decay of the parent [Ni(dpb)Cl] complex within ps has been determined through transient absorption spectroscopy (TAS) at ambient temperature (20 °C),[24] which agrees with our finding that [Ni(L^{Bn})Cl] is non-emissive in solution or in the solid at ambient temperature. However at low temperature, the lifetime of the excited state of [Ni(L^{Bn})Cl] might be prolonged compared with [Ni(dpb)Cl], which is probably due to the geometric peculiarities of [Ni(L^{Bn})Cl]. Unfortunately, TAS is not doable at low temperatures, impeding that we use this method to confirm the long lifetimes of [Ni(L^{Bn})Cl]. Unfortunately, the same is true for TAS in solid matrices. Nevertheless, in future work, we will search for a suitable matrix material to promote photoluminescence of the [Ni(L^{Bn})Cl] complex also at ambient temperature, which turned out to be very successful for the previously reported L^{NHR} derivatives, that showed phosphorescence in poly(methyl methacrylate) (PMMA) matrix in the temperature range between 6 K and 300 K.[29]

Conclusions

The N^C^N-cyclometalated complexes, [M(L^{Bn})Cl] (M = Pt, Pd, and Ni), featuring the 1,3-di(2-pyridyl)-benzene (HL^{Bn}) ligand benzyl substituted at both *ortho*-positions of the pyridyl units, were synthesised to generate a tight binding pocket for the Cl^- coligand (ancillary ligand). As expected, the complex geometries deviate from a perfect square planar coordination featuring C–M–Cl angles of around 150° for Pt(II) and Pd(II) and 139° for Ni(II) and τ_4 values of around 0.4. The photophysical studies show that the Pt(II) complex emits at RT in both solution and solid state. When incorporating into PMMA matrices at varying concentrations, the emission maximum shifted from 496 nm to 544 nm as the concentration increased from 0.5% to 5%. This shift as well as changes in the emission profile suggest the formation of emissive molecular aggregates. In contrast, the Pd(II) and Ni(II) complexes are non-emissive at RT due to faster non-radiative deactivation *via* MC states. At 77 K, all three complexes exhibit emission, with Pt(II) and Pd(II) showing the typical patterns for triplet emission from mixed ^{3}LC/^{3}MLCT states and emission maxima at around 500 nm. For the sample of the Ni(II) complex we found an unusual broad emission at around 700 nm with a particularly high quantum yield of 20% and a lifetime in the ms range. Such long-lived photoluminescence has been previously reported for similar [Ni(N^C^N)X] complexes (X = anionic ancillary ligands), but assignment to emission from excited triplet states is challenged by the inherent instability of these complexes towards hydrolysis. Assuming that the emission stems from the intact complexes and not from hydrolysis products would confirm that the rigidified structure in this complex leads to a reduced rate of non-radiative deactivation at low temperatures.

Comparing our findings with the previously studied [M(L^{NHR})Cl] complexes featuring similar rigidification through M–Cl···H–N hydrogen bonds, it is evident that while hydrogen bonding has been shown to stabilise the excited states and potentially foster photoluminescence in Ni(II) systems, the new approach using steric bulk alone can also minimise excited state distortions to some degree and thus enhance geometric similarity between ground and excited states. However, this rigidification seems to have only a positive impact on the photoluminescence of corresponding Ni(II) complexes, while for the Pd(II) derivatives no such effects were observed, which might be correlated to the less pronounced geometric distortion. In any case, and regardless of the still open question if the ms emission is photoluminescence from the studied Ni(II) complexes, the present study confirms that modifications in the second coordination sphere, whether through noncovalent interactions like hydrogen bonding or through steric effects,

can play a critical role in controlling the photophysical behaviour of transition metal complexes. Future work will continue to explore these strategies, investigating how different types of steric and electronic modifications influence the excited state behaviour and photophysical properties of such square-planar configured Ni(II), Pd(II), and Pt(II) complexes. Together with approaches to stabilise the Ni(II) derivatives against hydrolysis, this might ultimately lead to triplet photoluminescent Ni(II)-based materials.

Author contributions

M. N. investigation, visualisation, and writing – original draft; I. M. investigation, visualisation; C. A. S. conceptualisation, instrumentation, funding acquisition, supervision; P. G. H. instrumentation, supervision; A. K. conceptualisation, instrumentation, funding acquisition, supervision, visualisation, and writing, review & editing.

Conflicts of interest

There are no conflicts to declare.

Data availability

Information on the syntheses of the ligands with their analytical characterisation is available together with figures showing NMR, MS, UV-vis absorption, UV-vis emission spectra, cyclic voltammograms, tables with pertinent experimental and DFT-calculated data (pdf), and DFT-optimised molecular structure data (XYZ) are included in the SI. See DOI: **https://doi.org/10.1039/d5dt01385b**.

CCDC 2307143, 2271328 and 2258876 contains the supplementary crystallographic data for this paper.[65a–c]

Acknowledgements

We thank the German Academic Exchange Service (DAAD) (grant no. 57507871), the Deutsche Forschungsgemeinschaft [DFG Priority Programme 2102 "Light-controlled Reactivity of Metal Complexes" STR 1186/6-1 and 6-2 (C. A. S) as well as KL1194/16-1 and 16-2 (A. K.)] and the University of Cologne, EUniWell programme (EUniWell Abroad Fellowship 2022 for M. N.) for funding of this project. P. G. H acknowledges grant no. PID2021-122966NB-I00 funded by MCIN/AEI/10.13039/500100011033 and ERDF "A way of making Europe". C. A. S. gratefully acknowledges the generous financial support for the acquisition of an "Integrated Confocal Luminescence Spectrometer with Spatiotemporal Resolution and Multiphoton Excitation" (DFG/Land NRW: INST 211/915-1 FUGG; DFG EXC1003: "Berufungsmittel"). We also like to thank the Regional Computing Center of the University of Cologne (RRZK) for providing computing time on the DFG-funded High Performance Computing (HPC) system CHEOPS as well as for the support. Thanks also to Rose Jordan who helped us with the crystal structure refinement.

References

1 V. W.-W. Yam and A. S.-Y. Law, Luminescent d^8 Metal Complexes of Platinum(II) and Gold(III): from Photophysics to Photofunctional Materials and Probes, *Coord. Chem. Rev.*, 2020, **414**, 213298, DOI: **10.1016/j.ccr.2020.213298**.

2 M. T. Walden, P. Pander, D. S. Yufit, F. B. Dias and J. A. G. Williams, Homoleptic Platinum(II) Complexes with Pyridyltriazole Ligands: Excimer-Forming Phosphorescent Emitters for Solution-Processed OLEDs, *J. Mater. Chem. C*, 2019, **7**, 6592–6606, DOI: **10.1039/C9TC00768G**.

3 C. Bizzarri, E. Spuling, D. M. Knoll, D. Volz and S. Bräse, Sustainable Metal Complexes for Organic Light-Emitting Diodes (OLEDs), *Coord. Chem. Rev.*, 2018, **373**, 49–82, DOI: **10.1016/j.ccr.2017.09.011**.

4 Y. Zhang, Y. Wang, J. Song, J. Qu, B. Li, W. Zhu and W.-Y. Wong, Near-Infrared Emitting Materials via Harvesting Triplet Excitons: Molecular Design, Properties, and Application in Organic Light Emitting Diodes, *Adv. Opt. Mater.*, 2018, **6**, 1800466, DOI: **10.1002/adom.201800466**.

5 C. Lee, R. Zaen, K.-M. Park, K. H. Lee, J. Y. Lee and Y. Kang, Blue Phosphorescent Platinum Complexes Based on Tetradentate Bipyridine Ligands and Their Application to Organic Light-Emitting Diodes (OLEDs), *Organometallics*, 2018, **37**, 4639–4647, DOI: **10.1021/acs.organomet.8b00659**.

6 A. Colombo, G. De Soricellis, C. Dragonetti, F. Fagnani, D. Roberto, B. Carboni, V. Guerchais, T. Roisnel, M. Cocchi, S. Fantacci, E. Radicchi and D. Marinotto, Introduction of a mesityl substituent on pyridyl rings as a facile strategy for improving the performance of luminescent 1,3-bis-(2-pyridyl)benzene platinum(II) complexes: a springboard for blue OLEDs, *J. Mater. Chem. C*, 2024, **12**, 9702–9715, DOI: **10.1039/d4tc01458h**.

7 F. Glaser and O. S. Wenger, Recent Progress in the Development of Transition-Metal Based Photoredox Catalysts, *Coord. Chem. Rev.*, 2020, **405**, 213129, DOI: **10.1016/j.ccr.2019.213129**.

8 J.-J. Zhong, C. Yang, X.-Y. Chang, C. Zou, W. Lu and C.-M. Che, Platinum(II) Photo-Catalysis for Highly Selective Difluoroalkylation Reactions, *Chem. Commun.*, 2017, **53**, 8948–8951, DOI: **10.1039/C7CC03823B**.

9 M. Parasram and V. Gevorgyan, Visible Light-Induced Transition Metal-Catalyzed Transformations: Beyond Conventional Photosensitizers, *Chem. Soc. Rev.*, 2017, **46**, 6227–6240, DOI: **10.1039/C7CS00226B**.

10 A. A. Eremina, M. A. Kinzhalov, E. A. Katlenok, A. S. Smirnov, E. V. Andrusenko, E. A. Pidko, V. V. Suslonov and K. V. Luzyanin, Phosphorescent Iridium(III) Complexes with Acyclic Diaminocarbene Ligands as Chemosensors for

Mercury, *Inorg. Chem.*, 2020, **59**, 2209–2222, DOI: 10.1021/acs.inorgchem.9b02833.

11 K. Li, G. S. M. Tong, Q. Wang, G. Cheng, W.-Y. Tong, W.-H. Ang, W.-L. Kwong and C.-M. Che, Highly Phosphorescent Platinum(II) Emitters: Photophysics, Materials and Biological Applications, *Chem. Sci.*, 2016, **7**, 1653–1673, DOI: 10.1039/C5SC03766B.

12 L. C.-C. Lee and K. K.-W. Lo, Shining New Light on Biological Systems: Luminescent Transition Metal Complexes for Bioimaging and Biosensing Applications, *Chem. Rev.*, 2024, **124**, 8825–9014, DOI: 10.1021/acs.chemrev.3c00629.

13 A. M. Prokhorov, T. Hofbeck, R. Czerwieniec, A. F. Suleymanova, D. N. Kozhevnikov and H. Yersin, Brightly Luminescent Pt(II) Pincer Complexes with a Sterically Demanding Carboranyl-Phenylpyridine Ligand: A New Material Class for Diverse Optoelectronic Applications, *J. Am. Chem. Soc.*, 2014, **136**, 9637–9642, DOI: 10.1021/ja503220w.

14 J. A. G. Williams, A. Beeby, E. S. Davies, J. A. Weinstein and C. Wilson, An Alternative Route to Highly Luminescent Platinum(II) Complexes: Cyclometalation with N^C^N-Coordinating Dipyridylbenzene Ligands, *Inorg. Chem.*, 2003, **42**, 8609, DOI: 10.1021/ic035083+.

15 B. Schulze, C. Friebe, M. Jäger, H. Görls, E. Birckner, A. Winter and U. S. Schubert, PtII Phosphors with Click-Derived 1,2,3-Triazole-Containing Tridentate Chelates, *Organometallics*, 2018, **37**, 145–155, DOI: 10.1021/acs.organomet.7b00777.

16 J. Kalinowski, V. Fattori, M. Cocchi and J. A. G. Williams, Light-emitting Devices Based on Organometallic Platinum Complexes as Emitters, *Coord. Chem. Rev.*, 2011, **255**, 2401–2425, DOI: 10.1016/j.ccr.2011.01.049.

17 M. Hruzd, N. le Poul, M. Cordier, S. Kahlal, J.-Y. Saillard, S. Achelle, S. Gauthier and F. Robin-le Guen, Luminescent cyclometalated alkynylplatinum(II) complexes with 1,3-di(pyrimidin-2-yl)benzene ligands: synthesis, electrochemistry, photophysics and computational studies, *Dalton Trans.*, 2022, **51**, 5546–5560, DOI: 10.1039/d1dt04237h.

18 N. Zhou, C. Zou, S. Suo, Y. Liu, J. Lin, X. Zhang, M. Shi, X. Chang and W. Lu, Aggregation of phosphorescent Pd(II) and Pt(II) complexes with lipophilic counter-anions in non-polar solvents, *Dalton Trans.*, 2023, **52**, 5503–5513, DOI: 10.1039/d2dt03415h.

19 I. Maisuls, C. Wang, M. E. Gutierrez Suburu, S. Wilde, C. G. Daniliuc, D. Brünink, N. L. Doltsinis, S. Ostendorp, G. Wilde, J. Kösters, U. Resch-Genger and C. A. Strassert, Ligand-controlled and Nanoconfinement-boosted Luminescence Employing Pt(II) and Pd(II) Complexes: from Color-tunable Aggregation-enhanced Dual Emitters towards Self-referenced Oxygen Reporters, *Chem. Sci.*, 2021, **12**, 3270–3281, DOI: 10.1039/D0SC06126C.

20 Ch. Zou, J. Lin, S. Suo, M. Xie, X. Chang and W. Lu, Palladium(II) *N*-heterocyclic Allenylidene Complexes with Extended Intercationic Pd···Pd Interactions and MMLCT Phosphorescence, *Chem. Commun.*, 2018, **54**, 5319–5322, DOI: 10.1039/C8CC01652F.

21 J. Moussa, K. Haddouche, L.-M. Chamoreau, H. Amouri and J. A. G. Williams, New N^C^N-coordinated Pd(II) and Pt(II) complexes of a tridentate N-heterocyclic carbene ligand featuring a 6-membered central ring: synthesis, structures and luminescence, *Dalton Trans.*, 2016, **45**, 12644–12648, DOI: 10.1039/c6dt02415g.

22 M. Niazi, I. Maisuls, C. A. Strassert and A. Klein, Molecular Rigidification of Cyclometalated N^C^N Pt(II)- and Pd(II)-Based Triplet Emitters, *Organometallics*, 2024, **43**, 1547–1556, DOI: 10.1021/acs.organomet.4c00121.

23 T. Eskelinen, S. Buss, S. K. Petrovskii, E. V. Grachova, M. Krause, L. Kletsch, A. Klein, C. A. Strassert, I. O. Koshevoy and P. Hirva, Photophysics and Excited State Dynamics of Cyclometalated [M(Phbpy)(CN)] (M = Ni, Pd, Pt) Complexes: A Theoretical and Experimental Study, *Inorg. Chem.*, 2021, **60**, 8777–8789, DOI: 10.1021/acs.inorgchem.1c00680.

24 T. Ogawa and O. S. Wenger, Nickel(II) Analogues of Phosphorescent Platinum(II) Complexes with Picosecond Excited-State Decay, *Angew. Chem., Int. Ed.*, 2023, **62**, e202312851, DOI: 10.1002/anie.202312851.

25 O. S. Wenger, Photoactive Complexes with Earth-Abundant Metals, *J. Am. Chem. Soc.*, 2018, **140**, 13522–13533, DOI: 10.1021/jacs.8b08822.

26 Y.-S. Wong, M.-Ch. Tang, M. Ng and V. W.-W. Yam, Toward the Design of Phosphorescent Emitters of Cyclometalated Earth-Abundant Nickel(II) and Their Supramolecular Study, *J. Am. Chem. Soc.*, 2020, **142**, 7638–7646, DOI: 10.1021/jacs.0c02172.

27 T. Ogawa, N. Sinha, B. Pfund, A. Prescimone and O. S. Wenger, Molecular Design Principles to Elongate the Metal-to-Ligand Charge Transfer Excited-State Lifetimes of Square-Planar Nickel(II) Complexes, *J. Am. Chem. Soc.*, 2022, **144**, 21948–21960, DOI: 10.1021/jacs.2c08838.

28 D. Moreth, M. V. Cappellari, A. Müller, A. Oster, D. Schwab, N. L. Doltsinis, C. A. Strassert and U. Schatzschneider, Luminescent N^C^N Pincer Ni(II), Pd(II), and Pt(II) Complexes with a Pendant Coumarin Group: The Role of Auxiliary Ligands and Environments, *Inorg. Chem.*, 2025, **64**, 4223–4235, DOI: 10.1021/acs.inorgchem.4c03773.

29 M. Niazi, I. Maisuls, S. A. Schäfer, A. Oster, L. Santiago Diaz, D. M. Guldi, N. L. Doltsinis, C. A. Strassert and A. Klein, Conformational Locking of the Geometry in Photoluminescent Cyclometalated N^C^N Ni(II) Complexes, *Molecules*, 2025, **30**, 1901, DOI: 10.3390/molecules30091901.

30 J. K. McCusker, Electronic Structure in the Transition Metal Block and its Implications for Light Harvesting, *Science*, 2019, **363**, 484–488, DOI: 10.1126/science.aav9104.

31 C. Wegeberg and O. S. Wenger, Luminescent First-Row Transition Metal Complexes, *JACS Au*, 2021, **1**, 1860–1876, DOI: 10.1021/jacsau.1c00353.

32 N. Vogt, A. Sandleben, L. Kletsch, S. Schäfer, M. T. Chin, D. A. Vicic, G. Hörner and A. Klein, Role of the X Coligands in Cyclometalated [Ni(Phbpy)X] Complexes (HPhbpy = 6-phenyl-2,2′-bipyridine), *Organometallics*, 2021, **40**, 1776–1785, DOI: 10.1021/acs.organomet.1c00237.

33 R. Carrasco, J. Cano, X. Ottenwaelder, A. Aukauloo, Y. Journaux and R. Ruiz-García, Molecular and Electronic Structure of Square-planar Nickel(II), Nickel(III) and Nickel (III) π-Cation Radical Complexes with a Tetradentate o-Phenylenedioxamidate Redox-Active Ligand, *Dalton Trans.*, 2005, 2527–2538, DOI: 10.1039/B502481A.

34 S. Blanchard, F. Neese, E. Bothe, E. Bill, T. Weyhermüller and K. Wieghardt, Square Planar vs Tetrahedral Coordination in Diamagnetic Complexes of Nickel(II) Containing Two Bidentate π-Radical Monoanions, *Inorg. Chem.*, 2005, **44**, 3636–3656, DOI: 10.1021/ic040117e.

35 D. J. MacDonald, Absorption Spectra of Square-planar Complexes of Ethylenebisbiguanide with Nickel(II) and Palladium(II), *Inorg. Chem.*, 1967, **6**, 2269–2270, DOI: 10.1021/ic50058a034.

36 D. Maganas, A. Grigoropoulos, S. S. Staniland, S. D. Chatziefthimiou, A. Harrison, N. Robertson, P. Kyritsis and F. Neese, Tetrahedral and Square Planar Ni $[(SPR_2)_2N]_2$ Complexes, R = Ph & iPr Revisited: Experimental and Theoretical Analysis of Interconversion Pathways, Structural Preferences, and Spin Delocalization, *Inorg. Chem.*, 2010, **49**, 5079–5093, DOI: 10.1021/ic100163g.

37 M. V. Kulikova, K. P. Balashev and Kh. Erzin, Synthesis and Photophysical Properties of a Series of Biscyclometalated Platinum(II) Complexes on the Basis of a Tridentate 2,6-Diphenylpyridine, *Russ. J. Gen. Chem.*, 2003, **73**, 1839–1845, DOI: 10.1023/B:RUGC.0000025140.64970.10.

38 W. Lu, M. C. W. Chan, K.-K. Cheung and C.-M. Che, π–π Interactions in Organometallic Systems. Crystal Structures and Spectroscopic Properties of Luminescent Mono-, Bi-, and Trinuclear Trans-cyclometalated Platinum(II) Complexes Derived from 2,6-Diphenylpyridine, *Organometallics*, 2001, **20**, 2477–2486, DOI: 10.1021/om0009839.

39 G. S.-M. Tong and C.-M. Che, Emissive or Nonemissive? A Theoretical Analysis of the Phosphorescence Efficiencies of Cyclometalated Platinum(II) Complexes, *Chem. – Eur. J.*, 2009, **15**, 7225–7237, DOI: 10.1002/chem.200802485.

40 S.-W. Lai, M. C.-W. Chan, T.-C. Cheung, S.-M. Peng and C.-M. Che, Probing d^8–d^8 Interactions in Luminescent Mono- and Binuclear Cyclometalated Platinum(II) Complexes of 6-Phenyl-2,2′-bipyridines, *Inorg. Chem.*, 1999, **38**, 4046–4055, DOI: 10.1021/ic990238s.

41 D. J. Cardenas, A. M. Echavarren and M. C. Ramirez de Arellano, Divergent Behavior of Palladium(II) and Platinum(II) in the Metalation of 1,3-Di(2-pyridyl)benzene, *Organometallics*, 1999, **18**, 3337–3341, DOI: 10.1021/om990125g.

42 *APEX4—Software Suite for Crystallographic Programs*, Bruker AXS, Inc., Madison, WI, USA, 2021.

43 G. M. Sheldrick, Crystal Structure Refinement with SHELXL, *Acta Crystallogr., Sect. C:Struct. Chem.*, 2015, **71**, 3–8, DOI: 10.1107/S2053229614024218.

44 O. V. Dolomanov, L. J. Bourhis, R. J. Gildea, J. A. Howard and H. Puschmann, OLEX2: a Complete Structure Solution, Refinement and Analysis Program, *J. Appl. Crystallogr.*, 2009, **42**, 339–341, DOI: 10.1107/S0021889808042726.

45 G. M. Sheldrick, A Short History of SHELX, *Acta Crystallogr., Sect. A: Found. Crystallogr.*, 2008, **64**, 112–122, DOI: 10.1107/S0108767307043930.

46 M. J. Frisch, G. W. Trucks, H. B. Schlegel, G. E. Scuseria, M. A. Robb, J. R. Cheeseman, G. Scalmani, V. Barone, G. A. Petersson, H. Nakatsuji, X. Li, M. Caricato, A. V. Marenich, J. Bloino, B. G. Janesko, R. Gomperts, B. Mennucci, H. B. Hratchian, J. V. Ortiz, A. F. Izmaylov, J. L. Sonnenberg, D. Williams-Young, F. Ding, F. Lipparini, F. Egidi, J. Goings, B. Peng, A. Petrone, T. Henderson, D. Ranasinghe, V. G. Zakrewski, J. Gao, N. Rega, G. Zheng, W. Liang, M. Hada, M. Ehara, K. Toyota, R. Fukuda, J. Hasegawa, M. Ishida, T. Nakajima, Y. Honda, O. Kitao, H. Nakai, T. Vreven, K. Throssell, J. A. Montgomery, J. E. Peralta, F. Ogliaro, M. J. Bearpark, J. J. Heyd, E. N. Brothers, K. N. Kudin, V. N. Staroverov, T. A. Keith, R. Kobayashi, J. Normand, K. Raghavachari, A. P. Rendell, J. C. Burant, S. S. Iyengar, J. Tomasi, M. Cossi, J. M. Millam, M. Klene, C. Adamo, R. Cammi, J. W. Ochterski, R. L. Martin, K. Morokuma, O. Farkas, J. B. Foresman and D. J. Fox, *Gaussian 16, Rev. A.03*, Gaussian, Inc., Wallingford, CT, 2016.

47 F. Weigend and R. Ahlrichs, Balanced Basis Sets of Split Valence, Triple Zeta Valence and Quadruple Zeta Valence Quality for H to Rn: Design and Assessment of Accuracy, *Phys. Chem. Chem. Phys.*, 2005, **7**, 3297–3305, DOI: 10.1039/b508541a.

48 D. Andrae, U. Häußermann, M. Dolg, H. Stoll and H. Preuss, Energy-adjusted Ab Initio Pseudopotentials for the Second and Third Row Transition Elements, *Theor. Chim. Acta*, 1990, **77**, 123–141, DOI: 10.1007/BF01114537.

49 V. N. Staroverov, G. E. Scuseria, J. Tao and J. P. Perdew, Comparative Assessment of a New Nonempirical Density Functional: Molecules and Hydrogen-bonded Complexes, *J. Chem. Phys.*, 2003, **119**, 12129–12137, DOI: 10.1063/1.1626543.

50 S. Grimme, J. Antony, S. Ehrlich and H. Krieg, A Consistent and Accurate Ab Initio Parametrization of Density Functional Dispersion Correction (DFT-D) for the 94 Elements H-Pu, *J. Chem. Phys.*, 2010, **132**, 154104, DOI: 10.1063/1.3382344.

51 S. Grimme, S. Ehrlich and L. Goerigk, Effect of the Damping Function in Dispersion Corrected Density Functional Theory, *J. Comput. Chem.*, 2011, **2011**, 1456–1465, DOI: 10.1002/jcc.21759.

52 M. Cossi, N. Rega, G. Scalmani and V. Barone, Energies, Structures, and Electronic Properties of Molecules in Solution with the C-PCM Solvation Model, *J. Comput. Chem.*, 2003, **24**, 669–681, DOI: 10.1002/jcc.10189.

53 V. Barone and M. Cossi, Quantum Calculation of Molecular Energies and Energy Gradients in Solution by a Conductor Solvent Model, *J. Phys. Chem. A*, 1998, **102**, 1995–2001, DOI: 10.1021/jp9716997.

54 F. Plasser, TheoDORE: A Toolbox for a Detailed and Automated Analysis of Electronic Excited State Computations, *J. Chem. Phys.*, 2020, **152**, 1–14, DOI: 10.1063/1.5143076.

55 A. Sandleben, N. Vogt, G. Hörner and A. Klein, Redox Series of Cyclometalated Nickel Complexes [Ni((R)Ph(R′)bpy)Br]$^{+/0/-/2-}$ (H–(R)Ph(R′)bpy = Substituted 6-Phenyl-2,2′-bipyridine), *Organometallics*, 2018, **37**, 3332–3341, DOI: **10.1021/acs.organomet.8b00559**.

56 E. W. Dahl and N. K. Szymczak, Hydrogen Bonds Dictate the Coordination Geometry of Copper: Characterization of a Square-Planar Copper(I) Complex, *Angew. Chem., Int. Ed.*, 2016, **55**, 3101–3105, DOI: **10.1002/anie.201511527**.

57 L. Kletsch, G. Hörner and A. Klein, Cyclometalated Ni(II) Complexes [Ni(N^C^N)X] of the Tridentate 2,6-di(2-pyridyl) phen-ide Ligand, *Organometallics*, 2020, **39**, 2820–2829, DOI: **10.1021/acs.organomet.0c00355**.

58 Z. Wang, E. Turner, V. Mahoney, S. Madakuni, T. Groy and J. Li, Facile Synthesis and Characterization of Phosphorescent Pt(N^C^N)X Complexes, *Inorg. Chem.*, 2010, **49**, 11276–11286, DOI: **10.1021/ic100740e**.

59 L. Kletsch, R. Jordan, A. S. Köcher, S. Buss, C. A. Strassert and A. Klein, Photoluminescence of Ni(II), Pd(II), and Pt(II) Complexes [M(Me_2dpb)Cl] Obtained from C-H Activation of 1,5-Di(2-pyridyl)-2,4-dimethylbenzene (Me_2dpbH), *Molecules*, 2021, **26**, 5051, DOI: **10.3390/molecules26165051**.

60 L. Payen, L. Kletsch, T. Lapi, M. Wickleder and A. Klein, C–H Metalation of Terpyridine Stereoisomers with Ni(II), Pd(II), and Pt(II), *Inorganics*, 2023, **11**, 174, DOI: **10.3390/inorganics11040174**.

61 R. Von der Stück, S. Schmitz and A. Klein, C-X vs C-H activation for the synthesis of the cyclometalated complexes [Pd(YPhbpy)X] (HPhbpy = 6-phenyl-2,2′-bipyridine; X/Y = (pseudo)halides), *Inorg. Chem. Res.*, 2021, **5**, 173–192, DOI: **10.22036/icr.2021.278938.1101**.

62 R. Von der Stück, M. Krause, D. Brünink, S. Buss, N. L. Doltsinis, C. A. Strassert and A. Klein, Luminescent Pd(II) Complexes of Tridentate^{-}C^N^N Aryl-pyridine-(benzo)thiazole Ligands, *Z. Anorg. Allg. Chem.*, 2022, **648**, e202100278, DOI: **10.1002/zaac.202100278**.

63 R. Jordan, I. Maisuls, S. S. Nair, B. Dietzek-Ivanšić, C. A. Strassert and A. Klein, Enhanced luminescence properties through heavy ancillary ligands in [Pt(C^N^C)(L)] complexes, L = $AsPh_3$ and $SbPh_3$, *Dalton Trans.*, 2023, **52**, 18220–18232, DOI: **10.1039/d3dt03225f**.

64 B. A. Goodman and J. B. Raynor, Electron Spin Resonance of Transition Metal Complexes, *Adv. Inorg. Chem. Radiochem.*, 1970, **13**, 135–362, DOI: **10.1016/S0065-2792(08)60336-2**.

65 (*a*) M. Niazi, I. Maisuls, C. A. Strassert, P. González-Herrero and A. Klein, CCDC 2307143 ([Pt(L^{Bn})Cl]): Experimental Crystal Structure Determination, 2025, DOI: **10.5517/ccdc.csd.cc2hfrzp**; (*b*) M. Niazi, I. Maisuls, C. A. Strassert, P. González-Herrero and A. Klein, CCDC 2271328 ([Pd(L^{Bn})Cl]): Experimental Crystal Structure Determination, 2025, DOI: **10.5517/ccdc.csd.cc2g7hnw**; (*c*) M. Niazi, I. Maisuls, C. A. Strassert, P. González-Herrero and A. Klein, CCDC 2258876([Ni(L^{Bn})Cl]·$\frac{1}{2}CH_2Cl_2$): Experimental Crystal Structure Determination, 2025, DOI: **10.5517/ccdc.csd.cc2ftjzs**.